Hybrid Beamforming Design for Beam-Hopping LEO Satellite Communications

Jing Wang *†, Chenhao Qi *† and Shui Yu ‡
*School of Information Science and Engineering, Southeast University, Nanjing, China
†National Mobile Communications Research Laboratory, Southeast University, Nanjing, China
‡Faculty of Engineering and Information Technology, University of Technology Sydney, Australia
Email: {wangjing12, qch}@seu.edu.cn, Shui.Yu@uts.edu.au

GLOBECOM 2023 - 2023 IEEE Global Communications Conference | 979-8-3503-1090-0/23/$31.00 ©2023 IEEE | DOI: 10.1109/GLOBECOM54140.2023.10436908

***Abstract*—Since the hybrid beamforming (HBF) can approach the performance of fully-digital beamforming (FDBF) with much lower hardware complexity, we investigate the HBF design for beam-hopping (BH) low earth orbit (LEO) satellite communications (SatComs). Aiming at maximizing the sum-rate of totally illuminated beam positions during the whole BH period, we consider joint beamforming and illumination pattern (BIP) design subject to the HBF constraints and sum-rate requirements. To address the nonconvexity of the HBF constraints, we temporarily replace the HBF constraints with the FDBF constraints. Then a joint FDBF and illumination pattern design scheme is proposed using random search and fractional programming (FP) methods. Based on the designed illumination patterns, we optimize the digital beamformers with the constrained analog beamformers by utilizing the FP methods, where a sum-rate maximization HBF scheme is proposed. Simulation results show that the proposed schemes can achieve satisfactory sum-rate performance for BH LEO SatComs.**

***Index Terms*—Beam-hopping, hybrid beamforming, illumination pattern, LEO satellite communications.**

I. Introduction

To achieve full coverage of spatial and terrestrial wireless communications, the upcoming sixth generation (6G) wireless communications integrating satellite communications (SatComs) will establish a fully connected wireless network. SatComs can provide seamless and stable wireless service to complement and extend terrestrial communications, and therefore can address the challenge of insufficient connectivity for remote areas such as deserts, mountains and oceans [1], [2]. Compared to medium earth orbit and geosynchronous earth orbit counterparts, the low earth orbit (LEO) satellites are proximal to the earth, with the advantages of low latency in wireless access, reduced energy for launching, and small power for signal transmission from the satellites to terrestrial receivers [3]. Therefore, LEO SatComs have received increasing attention and become hotspots of commercial investment. The companies such as SpaceX and Amazon, have already put forward their commercial LEO SatCom products including Starlink and Kuiper.

As one of the key technologies of LEO SatComs, beam-hopping (BH) has raised great interest from both academia and the industry, owing to its flexibility and low complexity for implementation [3], [4]. BH is also capable of achieving multi-beam coverage with improved resource utilization, by simultaneously activating a set of beams at each time slot in a designed illumination pattern and periodically repeating in the next BH time window. To reduce the inter-beam interference among illuminated beams in the same time slot, adjacent beams are not preferred by the BH [5]. Aiming at minimizing the interference-based penalty function, a dynamic BH scheme is proposed in conjunction with selective precoding [6].

Furthermore, beamforming has been widely adopted to achieve high data-rate for LEO SatComs. Compared to the fully-digital beamforming (FDBF) that achieves the satisfactory performance at the cost of very-high hardware complexity [7], [8], hybrid beamforming (HBF) is promising to balance the performance and hardware constraints, especially for the LEO SatComs with limited on-board resource [9]. To maximize the energy efficiency, a hybrid analog and digital precoding designing method is developed in the massive MIMO LEO SatCom systems [10].

By combining the advantages of the flexibility and high data-rate, the beamforming design is considered for SatComs with BH. To reduce the power consumption, compressed sensing is employed to design FDBF with BH [5]. To balance the data traffic among clusters where each cluster is formed by multiple beams, a joint optimization method of singular-value-decomposition FDBF and BH is proposed subject to the service requirement of each beam [11]. However, to the best knowledge of authors, so far there has been no work on HBF for LEO SatComs with BH.

In this paper, we investigate the HBF design for BH SatComs. Aiming at maximizing the sum-rate of totally illuminated beam positions during the whole BH period, we consider joint beamforming and illumination pattern (BIP) design subject to the HBF constraints and sum-rate requirements. To address the nonconvexity of the HBF constraints, we temporarily replace the HBF constraints with the FDBF constraints. Then a joint FDBF and illumination pattern design (FDBF-IPD) scheme is proposed using random search and fractional programming (FP) methods. Based on the designed illumination patterns, we optimize the digital beamformers with the constrained analog beamformers by utilizing the FP methods, where a sum-rate maximization HBF (SM-HBF) scheme is proposed.

Notations: Boldfaced lowercase and uppercase letters represent vectors and matrices, respectively. The conjugate, expectation, transpose, Hermitian transpose, Frobenius norm, and Kronecker product are denoted as $(\cdot)^*$, $\mathbb{E}(\cdot)$, $(\cdot)^{\mathrm{T}}$, $(\cdot)^{\mathrm{H}}$, $\|\cdot\|_2$, and $\otimes$, respectively. $\mathbb{C}$ represents the sets of complex-valued numbers. $\mathcal{M} \triangleq \{1, 2, ..., M\}$, $\mathcal{N} \triangleq \{1, 2, ..., N_{\mathrm{s}}\}$ and $\mathcal{N}_{\mathrm{BS}} \triangleq \{1, 2, ..., N_{\mathrm{BS}}\}$.

II. System Model

Consider a downlink LEO SatCom system, where the LEO satellite equipped with N_{BS} antennas can simultaneously generate K spot beams to illuminate K beam positions on the ground. To illuminate the total N_{s} beam positions, we use the BH, where each BH period includes M time slots. To guarantee that each beam position is illuminated at least once during each BH period, we require $KM \geq N_{\mathrm{s}}$. As illustrated in Fig. 1, the beam positions with different radius are determined according to the number of ground users and the service demand before performing the BH [12]. Note that the satellite works in the multicast mode and therefore different users located in the same beam position receive the same signal from the satellite.

To transmit K independent data streams at each time slot, the LEO satellite employs the HBF architecture equipped with N_{RF} RF chains, where $K \leq N_{\mathrm{RF}}$. The HBF architecture includes analog beamformer $\boldsymbol{F}_t \in \mathbb{C}^{N_{\mathrm{BS}} \times N_{\mathrm{RF}}}$ and digital beamformer $\boldsymbol{Q}_t \in \mathbb{C}^{N_{\mathrm{RF}} \times N_{\mathrm{s}}}$ for the tth time slot, respectively. Let $\boldsymbol{s} \in \mathbb{C}^{N_{\mathrm{s}}}$ denote a symbol vector transmitted by the LEO satellite. The received signal at the total N_{s} beam positions in the tth time slot can be expressed as

$$\boldsymbol{y}_t = \boldsymbol{H}\boldsymbol{F}_t\boldsymbol{Q}_t\boldsymbol{s} + \boldsymbol{z}, \ t \in \mathcal{M}, \tag{1}$$

where $\boldsymbol{z} \in \mathbb{C}^{N_{\mathrm{s}}}$ denotes an additive white Gaussian noise vector with $[\boldsymbol{z}]_n \sim \mathcal{CN}\left(0, \sigma^2\right)$, and $\boldsymbol{H} \in \mathbb{C}^{N_{\mathrm{s}} \times N_{\mathrm{BS}}}$ denotes the downlink SatCom channel matrix. Note that $\boldsymbol{H}$ is supposed to be the same during the whole BH period [6]. In fact, we have

$$\boldsymbol{H} \triangleq [\boldsymbol{h}_1^{\mathrm{T}}, \boldsymbol{h}_2^{\mathrm{T}}, \ldots, \boldsymbol{h}_{N_{\mathrm{s}}}^{\mathrm{T}}]^{\mathrm{T}}, \tag{2}$$

where $\boldsymbol{h}_n$ denotes the channel vector between the LEO satellite and the nth beam position for $n \in \mathcal{N}$. Specifically, $\boldsymbol{h}_n$ can be expressed as

$$\boldsymbol{h}_n = \sum\nolimits_{l=1}^{L_n} g_l^{(n)} \boldsymbol{v}^{\mathrm{H}}\left(N_{\mathrm{BS}}, \theta_l^{(n)}\right), \tag{3}$$

where L_n denotes the number of the channel paths. $\theta_l^{(n)}$ represents the angle-of-departure (AoD) of the lth channel path, for $l = 1, 2, ..., L_n$. $\boldsymbol{v}\left(N_{\mathrm{BS}}, \theta_l^{(n)}\right)$ denotes the array response vector given as

$$\boldsymbol{v}\left(N_{\mathrm{BS}}, \theta_l^{(n)}\right) = \frac{1}{\sqrt{N_{\mathrm{BS}}}}\left[1, e^{j\pi\theta_l^{(n)}}, ..., e^{j\pi(N_{\mathrm{BS}}-1)\theta_l^{(n)}}\right]^{\mathrm{T}}. \tag{4}$$

Note that $g_l^{(n)}$ represents the channel gain of the lth channel path obeying Rician fading distribution with Rician factor $\chi_l^{(n)}$

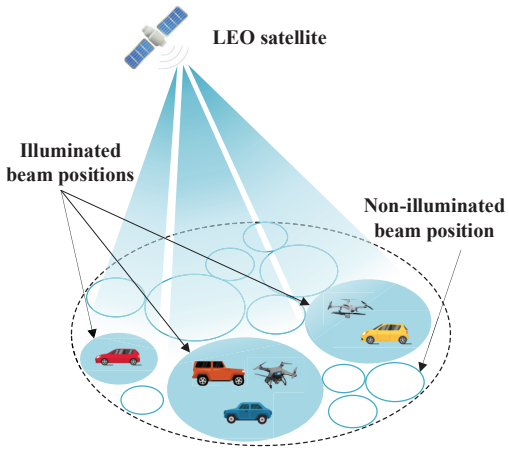

Fig. 1. Illustration of system model.

and $\mathbb{E}\left(\left|g_l^{(n)}\right|^2\right) = \eta_l^{(n)}$. Specifically, $\eta_l^{(n)}$ can be expressed as

$$\eta_l^{(n)} = \left(\frac{\lambda}{4\pi d}\right)^2 \frac{G_{\mathrm{r}} G_{\mathrm{t}}}{\kappa B T_{\mathrm{R}}}, \tag{5}$$

where B, λ, d, κ, and T_{R} represent the bandwidth, signal wavelength, propagation distance, Boltzmann's constant and receiving noise temperature, respectively. G_{r} and G_{t} denote the transmitting antenna gain of the satellite and receiving antenna gain of the ground users, respectively [9].

We denote a binary variable $x_{n,t} \in \{0, 1\}$ as the illumination indicator of the nth beam position in the tth time slot, for $t \in \mathcal{M}$ and $n \in \mathcal{N}$. If $x_{n,t} = 1$, the nth beam position is illuminated by a spot beam of the LEO satellite at the tth time slot; otherwise, it is not illuminated. Since the LEO satellite can simultaneously generate at most K spot beams in each time slot, we have

$$\sum\nolimits_{n=1}^{N_{\mathrm{s}}} x_{n,t} \leq K. \tag{6}$$

We define the illumination pattern as $\boldsymbol{X}$, where

$$[\boldsymbol{X}]_{n,t} \triangleq x_{n,t}, \ n \in \mathcal{N}, \ t \in \mathcal{M}. \tag{7}$$

To simplify the notation, we define

$$\boldsymbol{Q}_t \triangleq [\boldsymbol{q}_1^t, \boldsymbol{q}_2^t, \ldots, \boldsymbol{q}_{N_{\mathrm{s}}}^t]. \tag{8}$$

Then, the achievable rate of the nth beam position in the tth time slot can be expressed as

$$R_{n,t}\left(\boldsymbol{F}_t, \boldsymbol{Q}_t, \boldsymbol{X}\right) = \log_2\left(1 + \frac{x_{n,t}|\boldsymbol{h}_n\boldsymbol{F}_t\boldsymbol{q}_n^t|^2}{\sum_{k\neq n}^{N_{\mathrm{s}}} x_{k,t}|\boldsymbol{h}_n\boldsymbol{F}_t\boldsymbol{q}_k^t|^2 + \sigma^2}\right). \tag{9}$$

III. Joint Beamforming and Illumination Pattern Design

To maximize the sum-rate of the total N_{s} beam positions during the whole BH period, we jointly optimize the analog and digital beamforming matrices $\{\boldsymbol{F}_t, \boldsymbol{Q}_t, t \in \mathcal{M}\}$ together with the illumination pattern. The joint BIP design problem

can be formulated as

$$\max_{\boldsymbol{X},\{\boldsymbol{F}_t,\boldsymbol{Q}_t,t\in\mathcal{M}\}} \sum_{n=1}^{N_\mathrm{s}}\sum_{t=1}^{M} R_{n,t}\left(\boldsymbol{F}_t,\boldsymbol{Q}_t,\boldsymbol{X}\right) \tag{10a}$$

$$\text{s.t.} \quad \sum_{t=1}^{M} R_{n,t}\left(\boldsymbol{F}_t,\boldsymbol{Q}_t,\boldsymbol{X}\right)\geq\gamma_n,\forall n\in\mathcal{N}, \tag{10b}$$

$$\sum_{n=1}^{N_\mathrm{s}}\left\|\boldsymbol{F}_t\boldsymbol{q}_n^t\right\|_2^2\leq P_\mathrm{tot},\forall t\in\mathcal{M}, \tag{10c}$$

$$\left|\boldsymbol{F}_t\left(i,n\right)\right|=1,\forall i\in\mathcal{N}_\mathrm{BS},n\in\mathcal{N}, \tag{10d}$$

$$\sum\nolimits_{n=1}^{N_\mathrm{s}} x_{n,t}\leq K,\forall t\in\mathcal{M}, \tag{10e}$$

$$x_{n,t}\in\left\{0,1\right\},\forall n\in\mathcal{N},\forall t\in\mathcal{M}, \tag{10f}$$

where γ_n and P_tot are the predefined threshold of the sum-rate and the power constraint, respectively. To be specific, constraint (10b) indicates that the sum-rate of the nth beam position during the whole BH period is no smaller than γ_n. Constraint (10c) indicates that the total transmit power of the LEO satellite in each time slot is no larger than P_tot. Constraint (10d) indicates the unit-modulus constraints of analog beamformers. Constraint (10e) indicates that the maximum number of illuminated beam positions in each time slot is no larger than K. In fact, the constraints (10c), (10d) and (10e) compose the HBF constraints.

It is seen from (10a) and (10b) that the beamforming matrices and the illumination pattern are coupled, leading (10) to be a mixed integer non-convex optimization problem. To solve this joint BIP design problem, we temporarily replace the HBF constraints by the FDBF constraints. By solving the FDBF design problem in Section III-A, we can obtain an illumination pattern, which is used in Section III-B to design the HBF.

A. FDBF Design for BIP Problem

We define the fully-digital beamformer at the tth time slot for $t\in\mathcal{M}$ as

$$\boldsymbol{P}_t\triangleq[\boldsymbol{p}_1^t,\boldsymbol{p}_2^t,\ldots,\boldsymbol{p}_{N_\mathrm{s}}^t]\in\mathbb{C}^{N_\mathrm{BS}\times N_\mathrm{s}}. \tag{11}$$

We temporarily replace the HBF constraints on $\boldsymbol{F}_t$ and $\boldsymbol{Q}_t$, by the FDBF constraints on $\boldsymbol{P}_t$. Then the fully-digital BIP design problem can be given as

$$\max_{\boldsymbol{X},\{\boldsymbol{P}_t,t\in\mathcal{M}\}} \sum_{n=1}^{N_\mathrm{s}}\sum_{t=1}^{M} R_{n,t}\left(\boldsymbol{P}_t,\boldsymbol{X}\right) \tag{12a}$$

$$\text{s.t.} \quad \sum_{t=1}^{M} R_{n,t}\left(\boldsymbol{P}_t,\boldsymbol{X}\right)\geq\gamma_n,\forall n\in\mathcal{N}, \tag{12b}$$

$$\sum_{n=1}^{N_\mathrm{s}}\left\|\boldsymbol{p}_n^t\right\|_2^2\leq P_\mathrm{tot},\forall t\in\mathcal{M}, \tag{12c}$$

$$\text{(10e)},\text{(10f)}. \tag{12d}$$

Due to the binary property of $\boldsymbol{X}$, (12) is an integer programming problem, which is difficult to solve.

Suppose the candidate illumination patterns are denoted by a set $\{\mathcal{X}_i,i\in\mathcal{I}\}$, where I is the number of candidate illumination pattern sets and $\mathcal{I}\triangleq\{1,2,...,I\}$. To reduce the complexity of exhaustive search, we generate $\{\mathcal{X}_i,i\in\mathcal{I}\}$ obeying the following two criteria.

- To completely utilize the resource in each time slot, we simultaneously illuminated K beams in the tth time slot, i.e., replacing the inequality by the equality in (10e) as

$$\sum_{n=1}^{N_\mathrm{s}} x_{n,t}=K,\forall t\in\mathcal{M}. \tag{13}$$

- To avoid the redundant illumination, the nth beam position can only be illuminated once during the whole BH period, which can be expressed as

$$\sum_{t=1}^{M} x_{n,t}=1,\ \forall n\in\mathcal{N}. \tag{14}$$

The index set of non-illuminated beam positions at the tth time slot, denoted as $\mathcal{B}$, is initialized to be $\mathcal{N}$. The index set of illuminated beam positions at the tth time slot, denoted as $\mathcal{A}_t$, is determined by randomly choosing K beam positions from $\mathcal{B}$. At the next time slot, we update $\mathcal{B}$ by removing the beam positions of $\mathcal{A}_t$ from $\mathcal{B}$, which can be expressed as

$$\mathcal{B}\leftarrow\mathcal{B}\setminus\mathcal{A}_t. \tag{15}$$

By repeating (15), we determine $\mathcal{A}_t$ for $t=1,2,\ldots,M$. Then we can determine $\boldsymbol{X}$ by

$$x_{n,t}=\begin{cases}1, & n\in\mathcal{A}_t,t\in\mathcal{M}\\ 0, & \text{otherwise}\end{cases}. \tag{16}$$

Since $\boldsymbol{X}$ satisfies (13) and (14), it is a valid candidate illumination pattern, which can be added to $\{\mathcal{X}_i,i\in\mathcal{I}\}$ by

$$\mathcal{X}_i\leftarrow\boldsymbol{X},i\in\mathcal{I}. \tag{17}$$

In this way, we can determine $\{\mathcal{X}_i,i\in\mathcal{I}\}$, which is essentially based on the constrained random search. This part is summarized from step 4 to step 8 of **Algorithm 1**. In the following, based on the candidate illumination patterns, we will find one achieving the largest sum-rate.

Given $\boldsymbol{X}=\mathcal{X}_i,i\in\mathcal{I}$, we can rewrite (12) as

$$\max_{\{\boldsymbol{P}_t,t\in\mathcal{M}\}} \sum_{n=1}^{N_\mathrm{s}}\sum_{t=1}^{M} R_{n,t}\left(\boldsymbol{P}_t,\boldsymbol{X}\right) \tag{18a}$$

$$\text{s.t.} \quad \sum_{t=1}^{M} R_{n,t}\left(\boldsymbol{P}_t,\boldsymbol{X}\right)\geq\gamma_n,\forall n\in\mathcal{N}, \tag{18b}$$

$$\sum_{n=1}^{N_\mathrm{s}}\left\|\boldsymbol{p}_n^t\right\|_2^2\leq P_\mathrm{tot},\forall t\in\mathcal{M}, \tag{18c}$$

which is non-convex due to the logarithmic-fractional form of the objective function (18a) and constraint (18b). To deal with the non-convexity of (18), the FP method can be applied using the quadratic transform [13]. To simplify the notation,

we define

$$\widehat{\boldsymbol{P}}_k^t \triangleq \boldsymbol{p}_k^t \left(\boldsymbol{p}_k^t\right)^{\mathrm{H}}, k \in \mathcal{N}. \tag{19}$$

Then (18) can be transformed into

$$\max_{\substack{\{\boldsymbol{P}_t, t\in\mathcal{M}\},\\ \{\mu_{n,t}, t\in\mathcal{M}, n\in\mathcal{N}\}}} \sum_{n=1}^{N_{\mathrm{s}}}\sum_{t=1}^{M} f_{n,t}\left(\boldsymbol{p}_n^t, \mu_{n,t}\right) \tag{20a}$$

$$\text{s.t.} \quad \sum_{t=1}^{M} f_{n,t}\left(\boldsymbol{p}_n^t, \mu_{n,t}\right) \geq \gamma_n, \forall n \in \mathcal{N}, \tag{20b}$$

$$(18c), \tag{20c}$$

Note that a new function $f_{n,t}\left(\boldsymbol{p}_n^t, \mu_{n,t}\right)$ in (20) is defined as

$$f_{n,t}\left(\boldsymbol{p}_n^t, \mu_{n,t}\right) \triangleq \log_2\Big(1 + 2\mathrm{Re}\left\{\sqrt{x_{n,t}}\mu_{n,t}^{\mathrm{H}}\boldsymbol{h}_n\boldsymbol{p}_n^t\right\} - \mu_{n,t}^{\mathrm{H}}\Big(\sum\nolimits_{k\neq n}^{N_{\mathrm{s}}} x_{k,t}\boldsymbol{h}_n\widehat{\boldsymbol{P}}_k^t\boldsymbol{h}_n + \sigma^2\Big)\mu_{n,t}\Big), \tag{21}$$

where an auxiliary variable $\mu_{n,t}$ is defined as

$$\mu_{n,t} \triangleq \frac{\sqrt{x_{n,t}}\boldsymbol{h}_n^{\mathrm{H}}\boldsymbol{p}_n^t}{\sum_{k\neq n}^{N_{\mathrm{s}}} x_{k,t}\boldsymbol{h}_n^{\mathrm{H}}\widehat{\boldsymbol{P}}_k^t\boldsymbol{h}_n + \sigma^2}. \tag{22}$$

In fact, $\mu_{n,t}$ is determined by setting

$$\frac{\partial f_{n,t}\left(\boldsymbol{p}_n^t, \mu_{n,t}\right)}{\partial \mu_{n,t}} = 0. \tag{23}$$

Note that with a fixed $\mu_{n,t}$, (20) is convex, which is equivalent to (18) and can be solved by the interior-point method. By alternately updating $\mu_{n,t}$ with a fixed $\boldsymbol{p}_n^t$ and updating $\boldsymbol{p}_n^t$ with a fixed $\mu_{n,t}$, we run the iteration until triggering *Stop Condition 1*, which can be set as the maximum iteration numbers being reached. Then we can obtain a solution of $\boldsymbol{p}_n^t$ as

$$\overline{\boldsymbol{p}}_n^t = \arg\max_{\boldsymbol{p}_n^t} \sum_{n=1}^{N_{\mathrm{s}}}\sum_{t=1}^{M} f_{n,t}\left(\boldsymbol{p}_n^t, \mu_{n,t}\right). \tag{24}$$

Therefore, given $\mathcal{X}_i, i \in \mathcal{I}$, we can obtain $\overline{\boldsymbol{p}}_n^t$, $t = 1, 2, \ldots, M$, based on the procedures from (18) to (24). Then the designed beamforming matrix given $\mathcal{X}_i$ is denoted as

$$\overline{\boldsymbol{P}}_t^{(i)} \triangleq [\overline{\boldsymbol{p}}_1^t, \overline{\boldsymbol{p}}_2^t, \ldots, \overline{\boldsymbol{p}}_N^t]. \tag{25}$$

Then the optimized $\widetilde{\boldsymbol{X}}$ together with the designed fully-digital beamforming matrices $\widetilde{\boldsymbol{P}}_1, \widetilde{\boldsymbol{P}}_2, \ldots, \widetilde{\boldsymbol{P}}_M$ can be obtained by

$$[\widetilde{\boldsymbol{P}}_1, \widetilde{\boldsymbol{P}}_2, \ldots, \widetilde{\boldsymbol{P}}_M; \widetilde{\boldsymbol{X}}] = \arg\max_{\left\{\overline{\boldsymbol{P}}_1^{(i)}, \overline{\boldsymbol{P}}_2^{(i)}, \ldots, \overline{\boldsymbol{P}}_M^{(i)}; \mathcal{X}_i, i\in\mathcal{I}\right\}} \sum_{n=1}^{N_{\mathrm{s}}}\sum_{t=1}^{M} R_{n,t}\left(\overline{\boldsymbol{P}}_t^{(i)}, \mathcal{X}_i\right), \tag{26}$$

which achieves the largest sum-rate.

The proposed FDBF-IPD scheme is summarized in **Algorithm 1**. The computational complexity of the FDBF-IPD scheme is $O\left(JLN_{\mathrm{s}}{}^4(N_{\mathrm{s}}+M)^{1.5}\log_2(1/\zeta_1)\right)$, where L denotes the predefined maximum iteration numbers of *Stop Condition 1* and $\zeta_1 > 0$ is the solution accuracy [14].

Algorithm 1 FDBF-IPD Scheme

Input: N_{s}, N_{BS}, K, M and I.
Initialization: $\mathcal{B} \leftarrow \mathcal{N}$.
for $i = 1, 2, ..., I$ **do**
  for $t = 1, 2, ..., M$ **do**
    Obtain $\mathcal{A}_t$ applying randomized algorithm to $\mathcal{B}$.
    Update $\mathcal{B}$ via (15).
  end for
  Obtain $\mathcal{X}_i$ via (17).
  repeat
    Update $\{\mu_{n,t}, t \in \mathcal{M}, n \in \mathcal{N}\}$ via (22).
    Obtain $\overline{\boldsymbol{P}}_1^{(i)}, \overline{\boldsymbol{P}}_2^{(i)}, \ldots, \overline{\boldsymbol{P}}_M^{(i)}$ via (25).
  until *Stop Condition 1* is triggered
end for
Obtain optimized $\widetilde{\boldsymbol{P}}_1, \widetilde{\boldsymbol{P}}_2, \ldots, \widetilde{\boldsymbol{P}}_M$ and $\widetilde{\boldsymbol{X}}$ via (26).
Output: $\widetilde{\boldsymbol{P}}_1, \widetilde{\boldsymbol{P}}_2, \ldots, \widetilde{\boldsymbol{P}}_M$, $\widetilde{\boldsymbol{X}}$.

B. HBF Design for BIP Problem

Given the optimized $\widetilde{\boldsymbol{X}}$, we can reformulate (10) as

$$\max_{\{\boldsymbol{F}_t, \boldsymbol{Q}_t, t\in\mathcal{M}\}} \sum_{n=1}^{N_{\mathrm{s}}}\sum_{t=1}^{M} R_{n,t}\left(\boldsymbol{F}_t, \boldsymbol{Q}_t, \widetilde{\boldsymbol{X}}\right) \tag{27a}$$

$$\text{s.t.} \quad \sum_{t=1}^{M} R_{n,t}\left(\boldsymbol{F}_t, \boldsymbol{Q}_t, \widetilde{\boldsymbol{X}}\right) \geq \gamma_n, \forall n \in \mathcal{N}, \tag{27b}$$

$$\sum_{n=1}^{N_{\mathrm{s}}} \left\|\boldsymbol{F}_t\boldsymbol{q}_n^t\right\|_2^2 \leq P_{\mathrm{tot}}, \forall t \in \mathcal{M}, \tag{27c}$$

$$\left|\boldsymbol{F}_t\left(i,n\right)\right| = 1, \forall i \in \mathcal{N}_{\mathrm{BS}}, n \in \mathcal{N}, \tag{27d}$$

which is non-convex due to the coupled analog beamformer and digital beamformer in (27a)-(27c) and the unit-modulus constraint in (27d). To decouple (27), we generate a number of candidate sets of analog beamformers subject to the unit-modulus constraint, where each candidate set is used to design a candidate digital beamformer set by solving a sum-rate maximization problem subject to (27b) and (27c). Among all the candidate sets, we select one achieving the largest sum-rate.

Suppose there are G candidate sets of analog beamformers, denoted as $\{\mathcal{F}_g, g \in \mathcal{G}\}$, where $\mathcal{G} \triangleq \{1, 2, ..., G\}$. If $\boldsymbol{F}_1, \boldsymbol{F}_2, ..., \boldsymbol{F}_M$ satisfy

$$\left|\boldsymbol{F}_t\left(i,n\right)\right| = 1, \forall i \in \mathcal{N}_{\mathrm{BS}}, n \in \mathcal{N}, t \in \mathcal{M}, \tag{28}$$

they are valid candidate analog beamformers, which can be added to $\{\mathcal{F}_g, g \in \mathcal{G}\}$ by

$$\mathcal{F}_g \leftarrow \{\boldsymbol{F}_1, \boldsymbol{F}_2, ..., \boldsymbol{F}_M\}, g \in \mathcal{G}. \tag{29}$$

Given $\mathcal{F}_g, g \in \mathcal{G}$, the digital beamforming design subprob-

lem of (27) can be expressed as

$$\max_{\{\boldsymbol{Q}_t, t\in\mathcal{M}\}} \sum_{n=1}^{N_\mathrm{s}}\sum_{t=1}^{M} R_{n,t}\left(\boldsymbol{F}_t, \boldsymbol{Q}_t, \widetilde{\boldsymbol{X}}\right) \tag{30a}$$

$$\text{s.t.} \quad \sum_{t=1}^{M} R_{n,t}\left(\boldsymbol{F}_t, \boldsymbol{Q}_t, \widetilde{\boldsymbol{X}}\right) \geq \gamma_n, \forall n \in \mathcal{N}, \tag{30b}$$

$$\sum_{n=1}^{N_\mathrm{s}} \left\|\boldsymbol{F}_t \boldsymbol{q}_n^t\right\|_2^2 \leq P_\mathrm{tot}, \forall t \in \mathcal{M}. \tag{30c}$$

Similarly, the FP method can be applied to solve (30) using the quadratic transformation. Base on (8), we can transform (30) into

$$\max_{\substack{\{\boldsymbol{Q}_t, t\in\mathcal{M}\},\\ \{\eta_{n,t}, t\in\mathcal{M}, n\in\mathcal{N}\}}} \sum_{n=1}^{N_\mathrm{s}}\sum_{t=1}^{M} v_{n,t}\left(\boldsymbol{q}_n^t, \eta_{n,t}\right) \tag{31a}$$

$$\text{s.t.} \quad \sum_{t=1}^{M} v_{n,t}\left(\boldsymbol{q}_n^t, \eta_{n,t}\right) \geq \gamma_n, \forall n \in \mathcal{N}, \tag{31b}$$

$$\text{(30c)}, \tag{31c}$$

where a new function $v_{n,t}\left(\boldsymbol{q}_n^t, \eta_{n,t}\right)$ is defined in (30) at the bottom of this page, and

$$\eta_{n,t} \triangleq \frac{\sqrt{x_{n,t}}\boldsymbol{h}_n \boldsymbol{F}_t \boldsymbol{q}_n^t}{\sum_{k\neq n}^{N_\mathrm{s}} x_{k,t}\boldsymbol{h}_n \boldsymbol{F}_t \widehat{\boldsymbol{Q}}_k^t \boldsymbol{F}_t^\mathrm{H} \boldsymbol{h}_n^\mathrm{H} + \sigma^2}, \tag{31}$$

is defined as an auxiliary variable. Note that $\widehat{\boldsymbol{Q}}_k^t$ in (30) and (31) is defined as

$$\widehat{\boldsymbol{Q}}_k^t \triangleq \boldsymbol{q}_k^t \left(\boldsymbol{q}_k^t\right)^\mathrm{H}, k \in \mathcal{N}. \tag{32}$$

In fact, $\eta_{n,t}$ is determined by setting

$$\frac{\partial v_{n,t}\left(\boldsymbol{q}_n^t, \eta_{n,t}\right)}{\partial \eta_{n,t}} = 0. \tag{33}$$

With a fixed $\eta_{n,t}$, (31) is convex, which can be solved by the existing optimization toolbox. By alternately updating $\eta_{n,t}$ with a fixed $\boldsymbol{q}_n^t$ and updating $\boldsymbol{q}_n^t$ with a fixed $\eta_{n,t}$, we run the iterations until triggering *Stop Condition 2*, which can be set that the objective of (31) can no longer increase. Then we can obtain a solution of $\boldsymbol{q}_n^t$ as

$$\overline{\boldsymbol{q}}_n^t = \arg\max_{\boldsymbol{q}_n^t} \sum_{n=1}^{N_\mathrm{s}}\sum_{t=1}^{M} v_{n,t}\left(\boldsymbol{q}_n^t, \eta_{n,t}\right). \tag{34}$$

Therefore, given $\mathcal{F}_g$, $g \in \mathcal{G}$, we can obtain $\overline{\boldsymbol{q}}_n^t$, $t = 1, 2, \ldots, M$, and the designed digital beamforming matrix is

$$\overline{\boldsymbol{Q}}_t^{(g)} \triangleq [\overline{\boldsymbol{q}}_1^t, \overline{\boldsymbol{q}}_2^t, \ldots, \overline{\boldsymbol{q}}_N^t]. \tag{35}$$

By randomly generating G candidate sets of analog beamformers, we can obtain the corresponding digital beamformers and also their sum-rate. From them, we select one achieving the largest sum-rate with the corresponding M analog beamformers $\widetilde{\boldsymbol{F}}_1, \widetilde{\boldsymbol{F}}_2, \ldots, \widetilde{\boldsymbol{F}}_M$ and M digital beamformers $\widetilde{\boldsymbol{Q}}_1, \widetilde{\boldsymbol{Q}}_2, \ldots, \widetilde{\boldsymbol{Q}}_M$ by

$$[\widetilde{\boldsymbol{F}}_1, \widetilde{\boldsymbol{F}}_2, \ldots, \widetilde{\boldsymbol{F}}_M; \widetilde{\boldsymbol{Q}}_1, \widetilde{\boldsymbol{Q}}_2, \ldots, \widetilde{\boldsymbol{Q}}_M] = \arg \max_{\left\{\overline{\boldsymbol{Q}}_1^{(g)}, \overline{\boldsymbol{Q}}_2^{(g)}, \ldots, \overline{\boldsymbol{Q}}_M^{(g)}; \mathcal{F}_g, g\in\mathcal{G}\right\}} \sum_{n=1}^{N_\mathrm{s}}\sum_{t=1}^{M} R_{n,t}\left(\overline{\boldsymbol{Q}}_t^{(g)}, \mathcal{F}_g\right). \tag{36}$$

Note that as G grows to infinity, the globally optimal analog beamformers and digital beamformers can be obtained.

The detailed steps of proposed SM-HBF scheme are summarized in **Algorithm 2**. We can figure out that the computational complexity of the SM-HBF scheme is $O\left(G{N_\mathrm{s}}^4 (N_\mathrm{s}+M)^{1.5} \log_2(1/\zeta_2)\right)$, where $\zeta_2 > 0$ is the solution accuracy.

Algorithm 2 SM-HBF Scheme

Input: N_s, N_BS, K, M and G.
Obtain $\widetilde{\boldsymbol{X}}$ via **Algorithm 1**.
for $g = 1, 2, \ldots, G$ **do**
  for $t = 1, 2, \ldots, M$ **do**
    Randomly generate $\boldsymbol{F}_t$ based on (28).
  end for
  Obtain $\mathcal{F}_g$ via (29).
  repeat
    Update $\{\eta_{n,t}, t \in \mathcal{M}, n \in \mathcal{N}\}$ via (31).
    Obtain $\overline{\boldsymbol{Q}}_1^{(i)}, \overline{\boldsymbol{Q}}_2^{(i)}, \ldots, \overline{\boldsymbol{Q}}_M^{(i)}$ via (35).
  until *Stop Condition 2* is triggered
end for
Determine $\widetilde{\boldsymbol{F}}_1, \widetilde{\boldsymbol{F}}_2, \ldots, \widetilde{\boldsymbol{F}}_M, \widetilde{\boldsymbol{Q}}_1, \widetilde{\boldsymbol{Q}}_2, \ldots, \widetilde{\boldsymbol{Q}}_M$ via (36).
Output: $\widetilde{\boldsymbol{F}}_1, \widetilde{\boldsymbol{F}}_2, \ldots, \widetilde{\boldsymbol{F}}_M, \widetilde{\boldsymbol{Q}}_1, \widetilde{\boldsymbol{Q}}_2, \ldots, \widetilde{\boldsymbol{Q}}_M$.

IV. Simulation Results

We assume that the LEO satellite is equipped with $N_\mathrm{RF} = 6$ RF chains and $N_\mathrm{s} = 6$ beam positions, where the maximum number of illuminated beam positions is $K = 2$ and the number of BH time slots is $M = 3$. The channels between the LEO satellite and each beam position are supposed to include $L_n = 2$ channel paths, where the channel gain $g_l^{(n)}$ obeys Rician fading distribution with Rician factor $\chi_l^{(n)} = 10$ dB.

As shown in Fig. 2, for the proposed FDBF-IPD scheme, we evaluate the sum-rate of total N_s beam positions under different γ_n, N_BS and P_tot. For simplicity, we set γ_n the same for different n. It can be observed that as γ_n increases, the sum-rate of total N_s beam positions falls, which implies that high requirement of the sum-rate from the individual beam position results in a poor sum-rate of the total beam positions. Under the same γ_n and P_tot, a larger antenna array provides more beamforming design degrees of freedom and therefore

$$v_{n,t}\left(\boldsymbol{q}_n^t, \eta_{n,t}\right) \triangleq \log_2\Big(1 + 2\mathrm{Re}\left\{\sqrt{x_{n,t}}\eta_{n,t}^\mathrm{H}\boldsymbol{h}_n\boldsymbol{F}_t\boldsymbol{q}_n^t\right\} - \eta_{n,t}^\mathrm{H}\Big(\sum\nolimits_{k\neq n}^{N_\mathrm{s}} x_{k,t}\boldsymbol{h}_n\boldsymbol{F}_t\widehat{\boldsymbol{Q}}_n^t\boldsymbol{F}_t^\mathrm{H}\boldsymbol{h}_n^\mathrm{H} + \sigma^2\Big)\eta_{n,t}\Big). \tag{30}$$

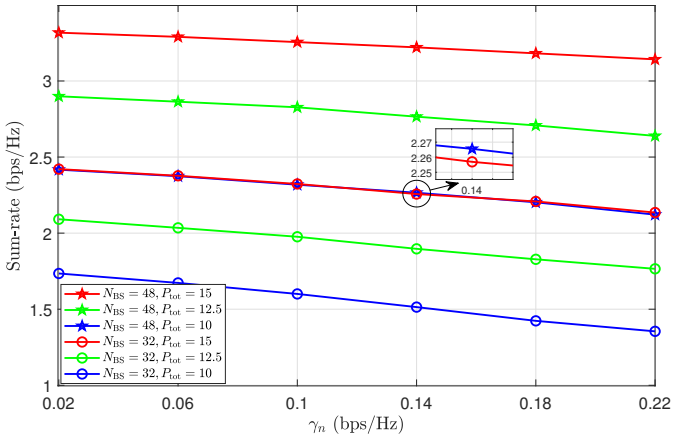

Fig. 2. Comparisons of sum-rate of total $N_{\rm s}$ beam positions under different γ_n for different $N_{\rm BS}$ and $P_{\rm tot}$.

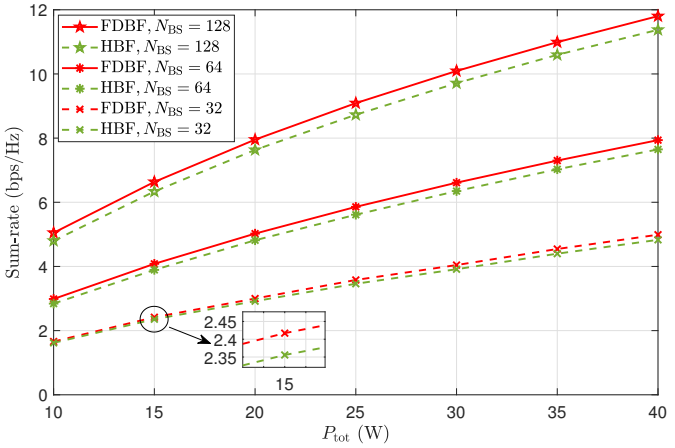

Fig. 3. Comparisons of sum-rate of total $N_{\rm s}$ beam positions under different $P_{\rm tot}$ for FDBF and HBF equipped with different $N_{\rm BS}$.

the sum-rate with $N_{\rm BS}=48$ is higher than that with $N_{\rm BS}=32$. When $P_{\rm tot}$ grows form 10 to 15, increased sum-rate can be achieved for the same γ_n and $N_{\rm BS}$.

Fig. 3 compares the sum-rate of total $N_{\rm s}$ beam positions for FDBF and HBF under different $P_{\rm tot}$ and $N_{\rm BS}$, where we fix $\gamma_n=0.1$ bps/Hz. It is seen that larger $P_{\rm tot}$ leads to higher sum-rate. To further evaluate the impact of different antenna numbers, we set $N_{\rm BS}=32$, 64 and 128 for both FDBF and HBF. When we enlarge $N_{\rm BS}$ from 32 to 128, increased sum-rate can be achieved for the same $P_{\rm tot}$. Furthermore, as $N_{\rm BS}$ increases, the gap between FDBF and HBF becomes large. The reason is that more antennas leads to more unit-modulus constraints coming from the phase shifters for HBF, which makes HBF more difficult to approach the performance of FDBF.

V. Conclusion

In this paper, we have investigated the HBF design for BH LEO SatComs. Aiming at maximizing the sum-rate of totally illuminated beam positions during the whole BH period, we have considered joint BIP design subject to the HBF constraints and sum-rate requirements. To address the nonconvexity of the HBF constraints, we have temporarily replaced the HBF constraints with the FDBF constraints. Then the FDBF-IPD scheme has been proposed using random search and FP methods. Based on the designed illumination patterns, we have optimized the digital beamformers with the constrained analog beamformers by utilizing the FP methods, where the SM-HBF scheme has been proposed. Simulation results have shown that the proposed schemes can achieve satisfactory sum-rate performance for BH LEO SatComs. Future work will be continued with the focus on the power allocation for BH LEO SatComs.

Acknowledgment

This work is supported in part by National Key Research and Development Program of China under Grant 2021YFB2900404.

References

[1] O. Kodheli, E. Lagunas, N. Maturo, S. K. Sharma, B. Shankar, J. F. M. Montoya, J. C. M. Duncan, D. Spano, S. Chatzinotas, S. Kisseleff, J. Querol, L. Lei, T. X. Vu, and G. Goussetis, "Satellite communications in the new space era: A survey and future challenges," *IEEE Commun. Surv. Tutor.*, vol. 23, no. 1, pp. 70–109, Oct. 2021.

[2] C. Qi and X. Wang, "Precoding design for energy efficiency of multibeam satellite communications," *IEEE Wirel. Commun. Lett.*, vol. 22, no. 9, pp. 1826–1829, Sep. 2018.

[3] X. Lin, S. Cioni, G. Charbit, N. Chuberre, S. Hellsten, and J.-F. Boutillon, "On the path to 6G: Embracing the next wave of low earth orbit satellite access," *IEEE Commun. Mag.*, vol. 59, no. 12, pp. 36–42, Dec. 2021.

[4] L. Lyu and C. Qi, "Beam position and beam hopping design for LEO satellite communications," *China Commun.*, vol. 20, no. 7, pp. 29–42, Jul. 2023.

[5] V. N. Ha, T. T. Nguyen, E. Lagunas, J. C. Merlano Duncan, and S. Chatzinotas, "GEO payload power minimization: Joint precoding and beam hopping design," in *Proc. IEEE Global Commun. Conf. (GLOBECOM)*, Dec. 2022, pp. 6445–6450.

[6] L. Chen, V. N. Ha, E. Lagunas, L. Wu, S. Chatzinotas, and B. Ottersten, "The next generation of beam hopping satellite systems: Dynamic beam illumination with selective precoding," *IEEE Trans. Wireless Commun.*, vol. 22, no. 4, pp. 2666–2682, Apr. 2023.

[7] H. Zhou, J. Li, K. Yang, H. Zhou, J. An, and Z. Han, "Handover analysis in ultra-dense LEO satellite networks with beamforming methods," *IEEE Trans. Veh. Technol.*, vol. 72, no. 3, pp. 3676–3690, Mar. 2023.

[8] C. Qi, Y. Yang, R. Ding, S. Jin, and D. Liu, "Multibeam satellite communications with energy efficiency optimization," *IEEE Wirel. Commun. Lett.*, vol. 26, no. 4, pp. 887–891, Apr. 2022.

[9] L. You, K.-X. Li, J. Wang, X. Gao, X.-G. Xia, and B. Ottersten, "Massive MIMO transmission for LEO satellite communications," *IEEE J. Sel. Areas Commun.*, vol. 38, no. 8, pp. 1851–1865, Aug. 2020.

[10] L. You, X. Qiang, K.-X. Li, C. G. Tsinos, W. Wang, X. Gao, and B. Ottersten, "Hybrid analog/digital precoding for downlink massive MIMO LEO satellite communications," *IEEE Trans. Wireless Commun.*, vol. 21, no. 8, pp. 5962–5976, Aug. 2022.

[11] C. Zhang, X. Zhao, and G. Zhang, "Joint precoding schemes for flexible resource allocation in high throughput satellite systems based on beam hopping," *China Commun.*, vol. 18, no. 9, pp. 48–61, Sep. 2021.

[12] C. Qi, H. Chen, Y. Deng, and A. Nallanathan, "Energy efficient multicast precoding for multiuser multibeam satellite communications," *IEEE Wirel. Commun. Lett.*, vol. 9, no. 4, pp. 567–570, Apr. 2020.

[13] K. Shen and W. Yu, "Fractional programming for communication systems—part ii: Uplink scheduling via matching," *IEEE Trans. Signal Process.*, vol. 66, no. 10, pp. 2631–2644, May. 2018.

[14] M. Grant and S. Boyd, "CVX: Matlab software for disciplined convex programming," http://stanford.edu/boyd/cvx, Jun. 2009.